Chemical Engineering Journal 160 (2010) 511–521

Contents lists available at ScienceDirect

Chemical Engineering Journal

journal homepage: www.elsevier.com/locate/cej

Hydrodynamic behavior analysis of a rotating disc contactor for aromatics extraction with 4-methyl-butyl-pyridinium·BF4 by CFD

Ferdy Onink[a,*], Christian Drumm[b], G. Wytze Meindersma[a], Hans-Jörg Bart[b], André B. de Haan[a]

[a] Eindhoven University of Technology, Eindhoven, Netherlands
[b] Lehrstuhl für Thermische Verfahrenstechnik, TU Kaiserslautern, Center of Mathematical and Computational Modeling, TU Kaiserslautern, P.O. Box 3049, 67653 Kaiserslautern, Germany

ARTICLE INFO

Article history:
Received 2 October 2009
Received in revised form 25 March 2010
Accepted 26 March 2010

Keywords:
Rotating disc contactor
CFD
Room temperature ionic liquids
Hydrodynamics
Hold-up
4-Methyl-N-butyl-pyridinium tetrafluoroborate
Aromatics extraction

ABSTRACT

An experimental and numerical simulation analysis of the hydrodynamic behavior for aromatics extraction with 4-methyl-N-butyl-pyridinium tetrafluoroborate is presented. Room temperature ionic liquids (RTILs) have proven to be promising solvents for the extraction of aromatic hydrocarbons, because of their non-volatile nature and their tailoring properties. The RTIL 4-methyl-N-butyl-pyridinium tetrafluoroborate ([4-mebupy]BF_4) was therefore tested as a solvent for the extraction of toluene from toluene/n-heptane in a rotating disc contactor (RDC). Hydrodynamic characteristics, like Sauter mean diameter and hold-up, were measured for different total fluxes and stirrer speeds. Unexpected behavior for the hold-up was observed in experiments when the RTIL was applied as solvent. At lower fluxes, the hold-up decreases with increasing rotor speed, when an increase of hold-up was expected. This behavior, however, can very well be explained by the existence of three operating regimes in the used RDC.

Computational fluid dynamics simulations of the two-phase flow in the RDC extractor have been performed to investigate the unexpected hold-up behavior. The numerical simulations were done using the commercial CFD software fluent, whereas an Euler–Euler model was applied together with the realizable k–ε turbulence model for the solution of the liquid–liquid problem. The numerical hold-up results are compared to the experimental profiles. Possible reasons for the hold-up anomalies, namely the path of the RTIL droplets as well as the velocity fields in both liquid phases, are presented and discussed. The work shows, that CFD can predict hydrodynamic characteristics even for extreme examples as in the present RTIL extraction.

1. Introduction

Room temperature ionic liquids (RTILs) are promising solvents for extraction processes [1–4]. The extractive separation of aromatic from aliphatic hydrocarbon is an important application in the petrochemical industry [5]. Current processes mostly use polar solvents such as sulfolane (UOP, SHELL [6]) and N-methyl pyrrolidone (Lurgi) [7]. RTILs are a new class of solvents and next to their almost negligible vapor pressure; they also offer the opportunity to be tailored for the targeted separation. With RTILs higher distribution ratios and selectivities are achieved compared to the common solvents used [8,9]. Of course, this has a major impact on the column design. Smaller columns can be used to achieve the requirements compared to the commonly used solvents. The main difference between RTILs and common solvents is their often considerably higher viscosity. For this reason, successful introduction of RTILs into extraction operations requires knowledge on their hydrodynamic characteristics in extraction equipment. Although the hydrodynamic behavior of classical solvents has been extensively studied [10–15], to our knowledge no studies have been reported for RTILs, except for our previous preliminary work [16,17]. In hydrodynamics, an important parameter determining the available mass transfer area is hold-up, the fraction of the active volume in an extraction column occupied by droplets of the dispersed phase [13]. For this study, we have selected a pilot plant rotating disc contactor (RDC) because it is the most commonly used extractor for aromatics extraction in the petrochemical industry [18]. As model system for the extraction of aromatic hydrocarbons from aliphatics, the extraction of toluene from a mixture with n-heptane with 4-methyl-N-butyl-pyridinium tetrafluoroborate ([4-mebupy]BF_4) as the solvent is chosen [19]. In this research, a RDC with five segments and eight compartments per segment is applied and experiments have been conducted to determine the hold-up and Sauter mean drop diameter as function of the flux and rotation speed. At the same time, an effort has been made to deepen the understanding of RTILs hydrodynamic behavior in an

* Corresponding author. Tel.: +31 620245608; fax: +31 402463966.
E-mail address: s.a.f.onink@tue.nl (F. Onink).

1385-8947/$ – see front matter © 2010 Elsevier B.V. All rights reserved.
doi:10.1016/j.cej.2010.03.062

Nomenclature

Symbols

C	constant
C_D	drag coefficient
d	droplet diameter
d_{32}	Sauter mean diameter
f	drag coefficient
F	interaction force
F	feed
g	gravity
G	turbulence production term
k	turbulent kinetic energy
K_d	distribution coefficient
n	number of droplets
p	pressure
Re	Reynolds number
S	strain rate
S	solvent
u	velocity
V	volume

Greek letters

α	volume fraction
ε	turbulent energy dissipation
μ	dynamic viscosity
μ_t	turbulent viscosity
ρ	density
σ	interfacial tension
τ	relaxation time
τ	shear stress

Subscripts

c,d	continuous and dispersed phase
l	liquid phase l
m	mixture
min	minimal

Abbreviations

CFD	computational fluid dynamics
RTIL	room temperature ionic liquid
RDC	rotating disc contactor
STD	standard deviation
rpm	revolutions per minute

RDC by predictive simulations using computation fluid dynamics (CFD).

In the field of liquid–liquid extraction, some good progress was made in determining column design parameters using CFD simulations. Flow fields and flow patterns in stirred RDC columns were studied both in single-phase [20,21] and two-phase operational mode [22,23]. Comparisons to experimental PIV (particle image velocimetry), LDV (laser doppler velocimetry) and LDA (laser doppler anemometer) data showed that CFD is a suitable design tool for the prediction of the hydrodynamic phenomena such as flow patterns, velocities, reversal vortices and backmixing [21,22,24]. Over the last years the Euler–Euler approach emerged as the standard approach to model multiphase problems and was successfully applied to model stirred RDC extractors of various geometries [22,23,25]. Generally, a two-fluid model is successfully applied for a two-phase problem, whereas the Sauter mean diameter represents the different sizes of the particles in the dispersed phase, while the influence of the size-specific terminal velocity resulting from the drop size distribution, could be neglected (e.g. [22,26]). For these reasons, the liquid–liquid flow is modeled using a Reynolds averaged turbulence model in conjunction with the Eulerian two-fluid equations for the hold-up simulations of the described system. In previous work, the simulated flow fields of the two-fluid model with constant d_{32} were compared to PIV measurements, taken on a pilot plant column, and agreed well with each other [22]. In the same work, the realizable k–ε model delivered the best results for the present two-phase flow [22]. The two-fluid model could also predict average volume fractions in one extraction compartment and single droplet terminal velocities in stagnant aqueous phase [27]. Governing equations are described in detail in the model section.

The paper is structured as follows: first the experiments and the governing CFD equations as well as the numerical scheme are introduced. After that, both experimental and numerical results are shown and compared to each other. Finally, the main conclusions are presented.

2. Experiments

2.1. Chemicals

The ionic liquid 4-methyl-N-butyl-pyridinium tetrafluoroborate (>97%), n-heptane (>99.9%) and toluene (>99.9%) were purchased from Merck and used without additional treatment.

2.2. Physical properties

Densities of the streams were measured at atmospheric pressure and at a temperature of 313 K using a density-meter Anton Paar DMA 5000 with a repeatability 1×10^{-6} g cm^{-3} and 0.001 °C. The cell of the density-meter was extensively cleaned and dried before each of the liquids was introduced. The density-meter was calibrated for the whole temperature range with a high purity water standard provided by Anton Paar. Each density measurement was repeated three times and the standard deviation (STD) was smaller than 2.0 kg m^{-3}.

The viscosities of the streams were measured at atmospheric pressure and a temperature of 313 K using an Ubbelohde viscometer, Schott, placed in a heated water bath. The time was measured using a digital stopwatch with precision of 10^{-3} s and each viscosity point was measured two times, the deviation between these two measurements was always <0.5%.

2.3. Analysis

Samples (for the extract phase approximately 0.5 mL and for the raffinate approximately 0.15 mL) were taken from both phases. 0.3 mL ethylbenzene was added to samples as the internal standard for GC analysis. Acetone (1.0 mL for the extract and 1.35 mL for the raffinate phase) was added to each sample to avoid phase splitting and to maintain a homogeneous mixture. The concentrations of toluene and n-heptane in the samples were analyzed by a Varian CP-3800 gas chromatograph with an Alltech Econo-Cap EC-Wax column (30 m × 0.32 mm × 0.25 μm) and with a Varian 8200 AutoSampler. Because the ionic liquid has no vapor pressure, it cannot be analyzed by GC. The RTIL was collected in a precolumn in order not to disrupt the analysis. The samples were analyzed in duple with a maximum deviation of <1%.

2.4. Experimental setup

The pilot RDC extraction column is schematically depicted in Figs. 1 and 2. The column consisted of five jacketed glass segments of each 360 mm in length and an inside diameter of 60 mm, with eight stirred compartments in each segment. Alternating glass

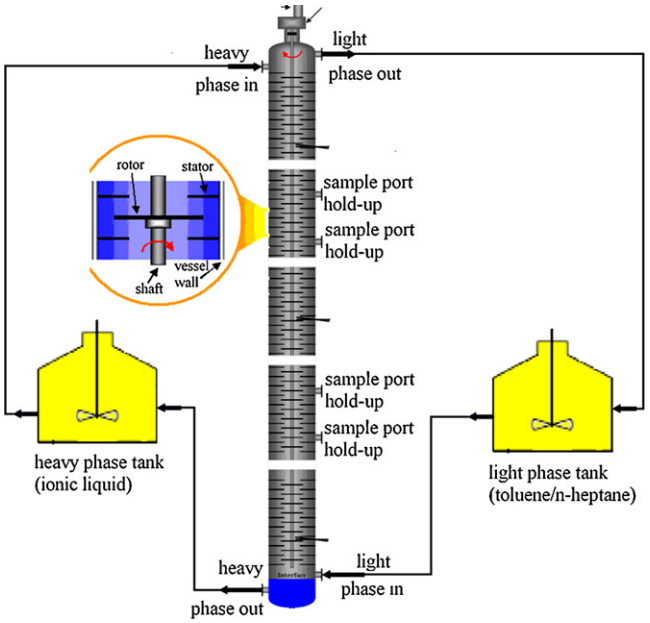

Fig. 1. Schematic representation of the rotating disc column being operated in recycle (hydrodynamic) mode.

segments had sample ports attached for measuring the hold-up. Settlers with a height of 240 mm (bottom) and 210 mm (top) with an internal diameter of 90 mm enclosed the stirred segments. The internals of the stirred segments consisted of alternating discs and doughnuts and were made of stainless steel. The outside diameter of the doughnuts was 60 mm, the inner 22 mm and the thickness was 1.5 mm. The discs had a diameter of 40 mm and a thickness of 1.5 mm. The distance between two doughnuts was 32 mm, equal to the distance between two discs. The RTIL solvent was fed to the top of the column and dispersed as the extract phase, which was collected from the bottom settler. The continuous n-heptane/toluene phase was fed from the bottom and the raffinate phase was collected from the top settler.

2.5. Hydrodynamic characteristics

For determination of the drop size and hold-up, the total flux and rotor speed were varied while keeping the solvent-to-feed (S/F) ratio constant. The minimum desired S/F ratio was calculated as:

$$\frac{S}{F_{\min}} \geq 1.5\frac{1}{K_d} \quad (1)$$

where S and F, respectively, are solvent and feed flow in kg/h; K_d is the weight-based distribution coefficient of toluene over the two-phases. Meindersma et al. [9] found for the weight-based distribution coefficient of toluene in [4-mebupy]BF_4 and n-heptane 0.20 for a concentration of 60 wt% toluene in n-heptane and thus the desired solvent-to feed ratio became 7.5.

When performing these hydrodynamic experiments, the system had to be operated in steady state and the phases had to be in equilibrium. The compositions and properties of the streams are shown in Table 1. To ensure equilibrium had been reached, the column was operated in recycle mode until no further change in the compositions of the streams could be noticed (Fig. 1). The flux (m^3/m^2 h) is defined as the volume that passes through the cross-section of the column in a certain time period. The drop sizes in the column were determined by taking digital photos of the column contents. The drop size was determined as the Sauter mean diameter as:

$$d_{32} = \frac{\sum n_i d_i^3}{\sum n_i d_i^2} \quad (2)$$

where n_i is the number of corresponding drop diameters, d_i is the measured drop diameter in meter. The mean average standard deviation for the drop sizes was 5%.

Hold-up is determined by taking 250 ml samples of the column content through the different sample ports at different heights in the column. These samples were collected in a separation funnel and were given a time to settle. The hold-up was then determined

Table 1
Pure components physical properties and composition and physical properties of streams at $T = 313$ K.

Component	Density (kg/m^3)	Viscosity (mPa s)
n-Heptane	669[a]	0.336[a]
Toluene	850[a]	0.467[a]
[4-Mebupy]BF_4	1179 ± 2	80.4 ± 0.05

	Composition/wt%				
Stream	Toluene	n-Heptane	[4-Mebupy]BF_4		
Raffinate	60 ± 3	40 ± 3		760 ± 1	0.389 ± 0.002
Extract	12 ± 1		88 ± 1	1150 ± 2	19.0 ± 0.05

[a] From Ref. [39].

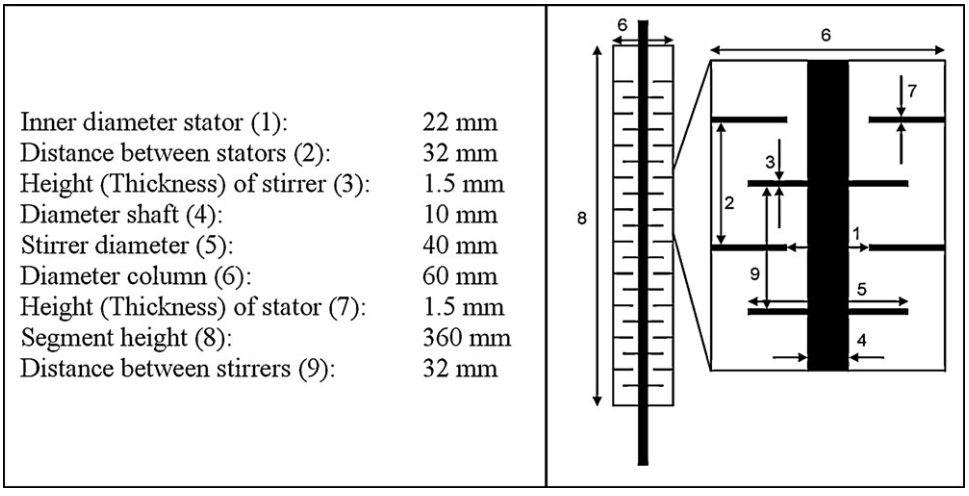

Fig. 2. Rotating disc contactor segment: geometry and dimensions.

by measuring the total volume and the dispersed phase volume as:

$$\phi = \frac{V_d}{V_d + V_c} \tag{3}$$

where V_d and V_c, respectively, are the volumes of the dispersed and continuous phases in mL. The error made in this determination is estimated as 10%.

3. CFD model

3.1. Mathematical model

The two-phase flow in the RDC extractor was modeled using the commercial CFD code Fluent 6.3. An Euler–Euler model where both phases are treated mathematically as interpenetrating continua was applied for the two-phase simulations of the extraction column. Coalescence and breakage events were ignored. The RTIL phase is in the form of spherical-dispersed droplets. The conservation equations are solved for each phase and can be written as follows:

Continuity (for the liquid phase l):

$$\frac{\partial(\alpha_l \rho_l)}{\partial t} + \nabla(\alpha_l \rho_l \vec{u}_l) = 0 \tag{4}$$

momentum (for phase l):

$$\frac{\partial(\alpha_l \rho_l \vec{u}_l)}{\partial t} + \nabla(\alpha_l \rho_l \vec{u}_l \vec{u}_l) - \nabla \tau_l = -\alpha_l \nabla p + \alpha_l \rho_l g + F_k \tag{5}$$

where α is the volume fraction, that represents the space occupied by each phase, ρ is the phase density, u is the phase velocity, τ is the stress–strain tensor, p is the pressure shared by all phases, g is the gravitational acceleration and F represents the interfacial forces. In addition to Eqs. (4) and (5) the constraint for the volume fractions must be satisfied:

$$\alpha_1 + \alpha_2 = 1 \tag{6}$$

The inter-phase interaction term F_k consists of different momentum exchange mechanisms. The work by Wang and Mao [26] showed that the drag force is the determining interaction force for liquid–liquid problems, while the lift force and the virtual mass force can be neglected. Therefore, only the drag force was taken into account as in our own previous work [22,27]. The drag force is then calculated as:

$$F_{c,d} = \frac{\rho_d \alpha_c \alpha_d f}{\tau_d}(\vec{u}_d - \vec{u}_c) \tag{7}$$

where the subscripts c and d stand for the two liquid phases, while f is the drag coefficient and τ_d the particulate relaxation time.

$$\tau_d = \frac{\rho_d d_d^2}{18 \mu_c} \tag{8}$$

In the above equation d_d is the Sauter mean diameter of the droplets of the dispersed liquid phase and μ is the dynamic viscosity. For the evaluation of the drag coefficient, the model of Schiller and Naumann (1935) is applied. The drag law can describe the rise velocities as a function of the drop size diameters as shown in previous work [27]:

$$f = \frac{C_D \ \mathrm{Re}}{24} \tag{9}$$

$$C_D = \begin{cases} \dfrac{24(1 + 0.15 \ \mathrm{Re}^{0.687})}{\mathrm{Re}} & \mathrm{Re} \le 1000 \\ 0.44 & \mathrm{Re} > 1000 \end{cases} \tag{10}$$

With the relative Reynolds number Re defined as:

$$\mathrm{Re} = \frac{\rho_c \left|\vec{u}_d - \vec{u}_c\right| d_d}{\mu_c} \tag{11}$$

The drag force (Eq. (7)) results finally in:

$$F_{c,d} = \frac{3 \rho_c \alpha_c \alpha_d C_D \left|\vec{u}_d - \vec{u}_c\right| (\vec{u}_d - \vec{u}_c)}{4 d_d} \tag{12}$$

For the calculation of the multiphase turbulence, the Fluent mixture turbulence model was used, which is an extension of the single-phase model. The turbulence is modeled through the realizable k–ε model [28]. The k–ε models generally include solving the transport equations separately for the turbulence kinetic energy k and its dissipation rate ε. The k and ε model equations are:

$$\frac{\partial}{\partial t}(\rho_m k) + \nabla(\rho_m \vec{u}_m k) = \nabla\left(\frac{\mu_{t,m}}{\sigma_k} \nabla k\right) + G_{k,m} - \rho_m \varepsilon \tag{13}$$

$$\frac{\partial}{\partial t}(\rho_m \varepsilon) + \nabla(\rho_m \vec{u}_m \varepsilon) = \nabla\left(\frac{\mu_{t,m}}{\sigma_k} \nabla \varepsilon\right) + \rho_m C_1 S \varepsilon - \rho_m C_2 \frac{\varepsilon^2}{k + \sqrt{\mu \varepsilon}} \tag{14}$$

$$C_1 = \max\left(0.43, \frac{\eta}{\eta + 5}\right) \tag{15}$$

$$\eta = S \frac{k}{\varepsilon} \tag{16}$$

where S is the strain rate tensor. G_k in Eq. (13) represents the generation of turbulent kinetic energy due to the mean velocity gradients. The density, velocity and turbulent viscosity of the mixture are:

$$\rho_m = \alpha_c \rho_c + \alpha_d \rho_d \tag{17}$$

$$\vec{u}_m = \frac{\alpha_c \rho_c \vec{u}_c + \alpha_d \rho_d \vec{u}_d}{\alpha_c \rho_c + \alpha_d \rho_d} \tag{18}$$

$$\mu_{t,m} = \rho_m C_\mu \frac{k^2}{\varepsilon} \tag{19}$$

Default values were used for the model constants C_1, C_2 and C_μ. Our own previous investigations lead to the conclusion that the current model is the most suitable available multiphase-model in Fluent for the description of the liquid–liquid flow [22]. The derivation of the conservation equations for mass and momentum for each of the both phases is done by ensemble averaging the local instantaneous balances.

3.2. Numerical procedure

All flow conditions as phase volume flows, stirrer speeds and Sauter mean diameters were the same as in the experiments. A 2D axis-symmetric grid of one segment (8 stirred compartments) was modeled in Gambit. Because of the rotational symmetry of a rotating disc contactor (Figs. 1 and 2), the 2D grid can be adopted without losing information. Previous work showed that a 2D grid delivers reliable results regarding the hydrodynamics of an RDC [22,27]. Quadrilateral elements with a grid space of 1.5 mm were adopted to map the flow domain (5000 cells). A part of the computational grid is depicted in Fig. 3. The complete grid represents one complete segment (see Fig. 2) and two settling zones (100 mm length) at the top and at the bottom. Standard wall functions modeled the near-wall region. Concerning the boundary conditions, the common approach with one pressure outlet condition at the top and one velocity-inlet at the bottom was applied. The surfaces of the rotating disc and the column wall were defined with no-slip wall boundary conditions. The simulations were carried out unsteadily using time steps between 0.01 and 0.001 s with the first order implicit solver. The QUICK scheme was used for the flow equations for the discretisation in space. The SIMPLE algorithm was used for the pressure–velocity coupling. Convergence of the solution was considered when the residual of the continuity equation is $>10^{-3}$.

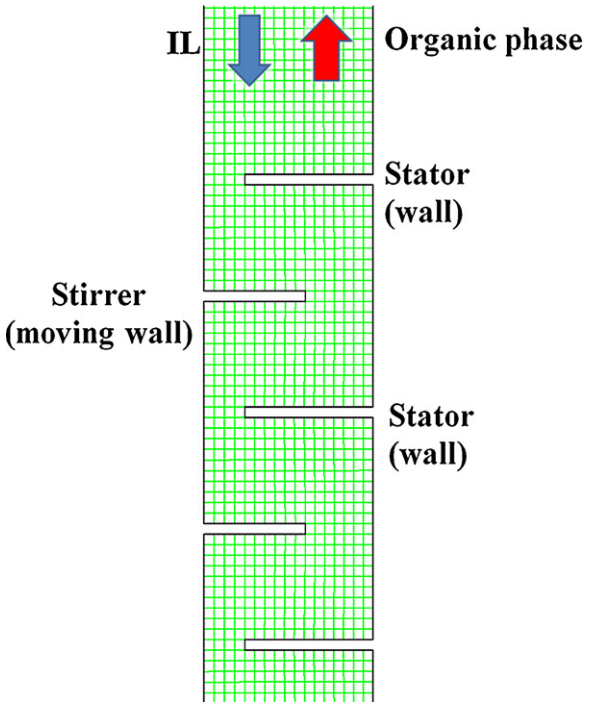

Fig. 3. Computational grid.

4. Results and discussion

4.1. Physical properties and analysis

As can be seen in Table 1, a large density difference exists between the raffinate and extract phase. According to Kumar and Hartland [29] (Eq. (20)), this encourages the formation of small droplets, which normally has a positive effect on the extraction efficiency.

$$d_{32} \propto \left(\frac{\rho_c}{\Delta\rho}\right)^{0.24} \tag{20}$$

On the other hand, the high viscosity of [4-mebupy]BF_4 (80.4 mPa s) could lead to formation of large droplets. The viscosity of the extract stream, however, is decreased from 80.4 to 19.0 mPa s due to the presence of 12 wt% toluene. Except for the viscosity of [4-mebupy]BF_4, the other physical properties of the system used are comparable to regular systems. Because this research only focuses on the hydrodynamic behavior without any mass transfer of the RDC, the compositions of both phases are constant over the height of the column.

4.2. Hold-up

The experimental hold-up fraction for constant flow rates of both phases vs. rotor speed is shown in Fig. 4. At a high flux of 10.5 m^3/m^2 h, the hold-up increases with increasing rotor speed as expected and as reported by others [30,31]. At lower fluxes, 8.2 and 3.7 m^3/m^2 h, the hold-up first decreases with increasing rotor speeds but when the rotor speed is increased further, the hold-up rises again with increasing rotor speed. Increasing rotor speeds generally results in the formation of smaller droplets and, hence, a decrease in velocity of the droplets, which in turn results in an increase in hold-up. Decrease of the hold-up with increasing rotor speeds, therefore, seems an anomaly, but is encountered more often in RDC's, as will be explained hereafter.

Vermijs and Kramers [32] did not discern this hold-up decrease for the hydrodynamic behavior of the RDC, which they used for extraction of acetic acid from methyl isobutyl ketone with water. However, rearrangement of their results shows a decreasing hold-up with increasing rotor speed up to rotor speeds of 600–800 rpm (Fig. 5), while there is an increase in hold-up with increasing rotor speed at higher fluxes. A decrease in hold-up with increasing rotor speed, up to rotor speeds of about 600–800 rpm, is also reported by Kamath et al. [33] for a system consisting of kerosene and water in a RDC with dimensions comparable to the one used in this research. At higher rotor speeds, above 600–800 rpm, the hold-up increases with increasing flux and this increase is larger at higher fluxes.

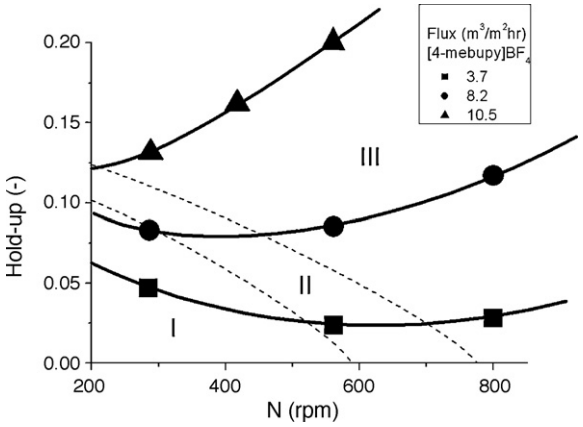

Fig. 4. Hold-up, as function of rotation speed at various fluxes, for extraction of toluene from n-heptane with [4-mebupy]BF_4 with $S/F = 7.5$ and $T = 313$ K, RDC being operated in recycle (hydrodynamic) mode, dashed lines represent operating regimes.

One can distinguish different working regimes for an RDC, as Kasatkin et al. [34] reported in analogy with the results of the hold-up profiles for other agitated contactors. For pulsed sieve-plate columns, Karr reciprocating-plate columns (KRPC) and for multistage vibrating disc contactor (MVDC), three regimes can be distinguished, respectively the mixer-settler, dispersion and finally the emulsion regime [13].

When operating a RDC in the first regime with increasing rotor speed, hold-up decreases. In the second regime, a transition regime, an increase of the rotor speed does not affect the hold-up. Finally, when being operated in the third regime, an increase of the rotor speed leads to an increase in the hold-up see Fig. 6.

The first regime is characterized as follows. At low rotor speeds, there is cohesion of the droplets at the stator ring and when the rotor speed is increased, the droplets at the stator ring tend to fall down through the column. Because there is an almost free fall of

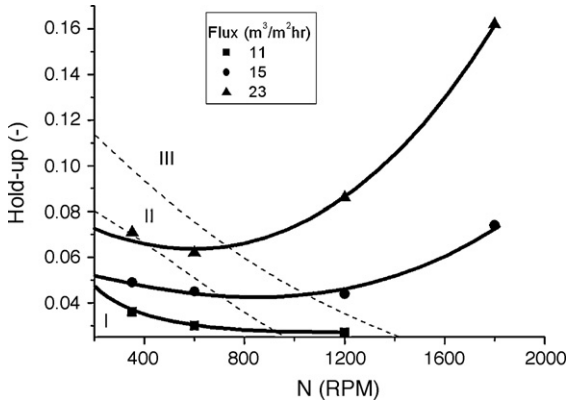

Fig. 5. Effect of rotor speed on hold-up for the system water–acetic acid–methyl isobutyl ketone at a constant solvent (water) to feed (MIBK) ratio of 1 with different fluxes [32].

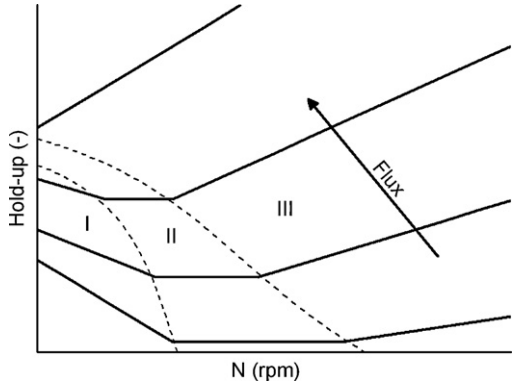

Fig. 6. Hydrodynamic operating regimes of a rotating disc extractor.

droplets of the dispersed phase, drops just fall faster if the rotor speed increases, causing a decrease in the hold-up. For the KRPC and MVDC this phenomenon is also observed when the column is operated at low levels of agitation in the mixer-settler or dispersion regime.

The third regime is revealed when an increase of the rotor speed leads to an increase in the hold-up. Comparable to the already mentioned KRPC and MVDC, being operated in the emulsion regime [13], an increase of the rotor speed leads to the formation of smaller droplets. Because the gravitational force on small droplets is smaller than for bigger droplets, the down coming velocity is lower for small drops, hence the hold-up increases.

The second regime is a transition state between the first and third regime. An increase of the rotor speed has no influence on the hold-up: the effect of the droplets falling down from the stator is compensated by the fact that the droplets become smaller and therefore their down coming velocity decreases. This regime corresponds to crowded settling of the droplets respectively the mixer-settler regime.

The clearly visible influence of the flux on the above mentioned phenomena will be explained in the next paragraph.

4.3. Drop size

Fig. 7 shows the results for drop size vs. rotor speed for the extraction of toluene from n-heptane for different fluxes. It is clear that, as expected, the drop size decreases with increasing rotor speed, because increasing rotor speed leads to an increase in

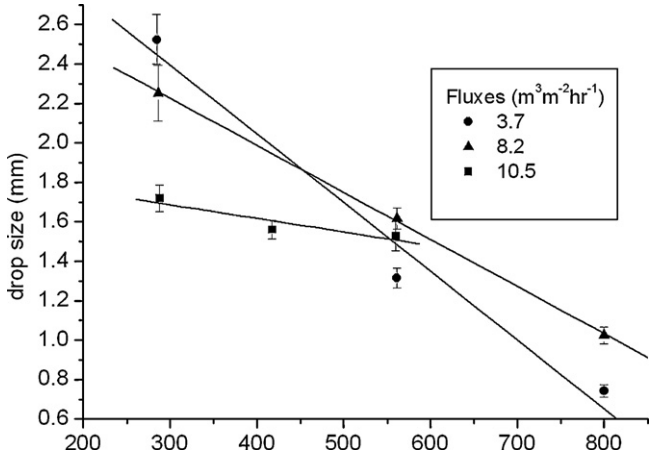

Fig. 7. Drop size, as function of rotation speed at various fluxes, for extraction of toluene from n-heptane with [4-mebupy]BF_4, with $S/F = 7.5$ and $T = 313$ K, RDC being operated in recycle (hydrodynamic) mode.

breakup of the droplets. In other words, an increase in the energy supplied by the rotors to the dispersed phase overcomes internal forces of the droplets and, therefore, they break up.

It can be seen from Fig. 7 that the influence of the rotor speed on the drop size is the largest for the lowest flux and that this influence decreases with increasing flux. At constant low flux, there exist relatively few but large droplets. Therefore, if the energy supplied by the rotor is increased, the size of the droplets decreases fast, because the energy dissipation is distributed over a small amount of droplets, in other words, this small amount of droplets experiences a relatively large shear force from the rotor.

As already stated above, at low flux and at low rotor speed, the size of the droplets is relatively large. When the flux is increased at constant low rotor speed, the size of the droplets decreases, as was also found by Al-Rahawi et al. [35]. This is caused by the fact that when the flux is increased, the dispersed phase droplets experience a higher shear force from the continuous phase leading to smaller droplets. The flux is defined as the sum of the flow of the dispersed and continuous phase, which are coupled via the solvent-to-feed ratio This ratio is kept constant at $1.5(S/F)_{min} = 7.5$.

If the flux is increased, the amount of the droplets is also increased, their size, however, being less influenced by an increase of the rotor speed than in the case for lower fluxes. The reason for this is the fact that the supplied energy now has to break up more droplets. From Fig. 8 can be seen that at a constant rotor speed of 560 rpm, but with increasing flux, accumulation of the dispersed phase at the stator increases. Therefore, the energy available per droplet, supplied by the shear force of the rotor, is decreased.

Now the occurrence of the operating regimes can be endorsed with the influence of the flux. At high flux, the column is operating fully in the third regime. Because of the high flux, the droplets are relatively small. So if the rotor speed is increased, smaller droplets are formed, their down coming velocity is decreased and the hold-up increases. For low fluxes, the column is being operated in the first regime for low rotor speeds. An increase of the rotor speed leads to a rapid decrease of the drop size, but because the fact that at low fluxes relatively a small amount of droplets is present, these droplets undergo less shear force from the continuous phase. Consequently, their down coming velocity is not affected by this shear force. Until a rotor speed of approximately 500 rpm for a flux of 3.7 and 300 rpm for a flux of 8.2 m^3/m^2 h, the column is being operated in the first regime (Fig. 6); the hold-up decreases with increasing rotor speeds. If rotor speeds exceed 700 rpm for a flux of 3.7 and 450 rpm for a flux of 8.2 m^3/m^2 h, the column is being operated in the third regime; the hold-up increases with increasing rotor speeds. Between 500 and 700 rpm for a flux of 3.7 and 300 and 450 rpm for a flux of 8.2 m^3/m^2 h, the column is being operated in the transition, second, regime.

4.4. CFD simulations

The hold-up results of the CFD simulations are presented and discussed in the following section. The simulated hold-up for the low flow rate (3.7 m^3/m^2 h) of both phases is shown in Fig. 9. One can see the path of the dispersed phase for a stirrer revolution of 285, 561 and 800 rpm through the compartment in Fig. 9. The same drop sizes are applied as determined from the experiments (2.52, 1.31 and 0.74 mm). The droplets do not penetrate the outer regions of the compartments and move mainly above stirrer and stator and near the stirrer shaft. The path of the RTIL droplets is straightforward through the compartment and almost not affected by the stirrers. Similar observations about the path and hold-up of the droplets were also made in experiments. It is also obvious that the hold-up of the RTIL decreases with increasing rotor speed. The simulated hold-up fraction for the low flow rate (3.7 m^3/m^2 h) is again depicted in Fig. 10, but now scaled from 0% to 10% volume frac-

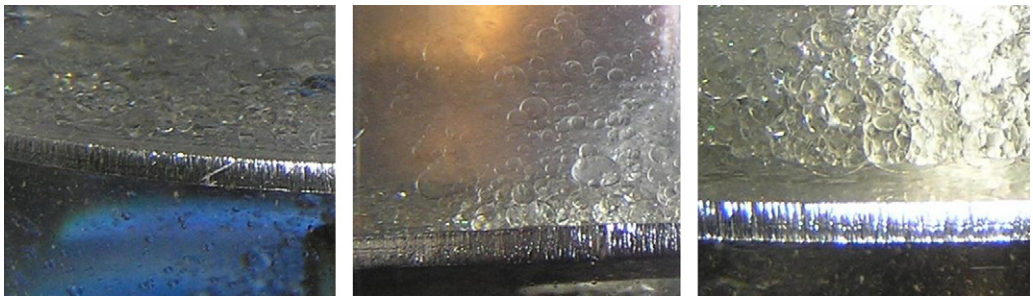

Fig. 8. Photographs of increase of dispersed phase at the stators with increasing fluxes (3.7–10.5 m^3/m^2 h) during hold-up experiments and at a rotor speed of 562 rpm.

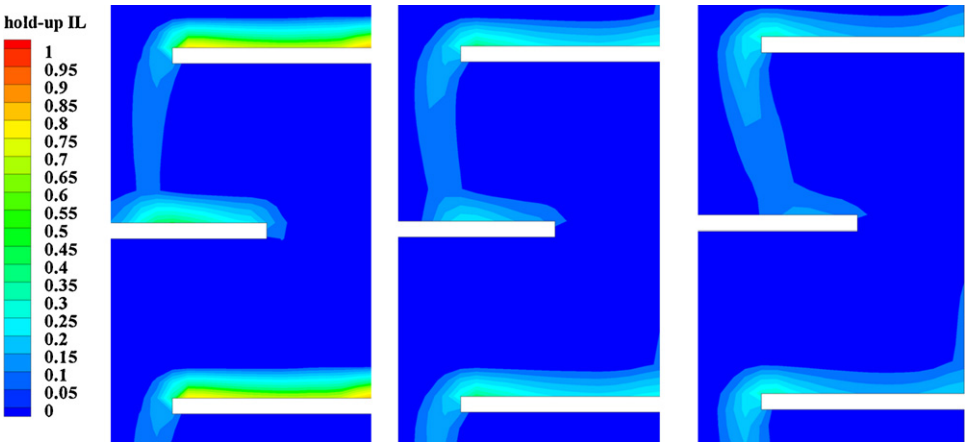

Fig. 9. Simulated hold-up of the RTIL as a function of rotation speed (280–562–800 rpm) at flux 3.7 m^3/m^2 h.

tion to resolve the small volume fractions better. It seems that the smaller droplets are swept out more easily resulting in less hold-up above stirrers and stators. Although the volume fraction near the stirrer tip towards the column wall increases and the droplets penetrate the region between the stators slightly more with higher stirrer speed, the higher stirrer speed cannot account for a higher hold-up. The same trend as before is also visible in Fig. 10. The average volume fraction in one compartment for 285 rpm is around 3.6% and reduces to 2.2% for 800 rpm.

In Figs. 11–13, the velocity vectors and contours of the organic and dispersed RTIL phase for the low flow rate (3.7 m^3/m^2 h) as a function of stirrer revolution are shown. Contours of the axial velocity and velocity vectors of the RTIL phase are depicted in Fig. 11, while Fig. 12 focuses on the contours of the radial velocity. It is obvious from Figs. 11 and 12 that the main direction of the velocity vectors is in the axial direction to the bottom of the column, which represents the main part of the RTIL velocity. The higher stirrer revolution accounts for a lower axial velocity in the regions between the stirrers and stators on one hand (see Fig. 11), but accounts also for a higher radial velocity at the stirrer and above the stators on the other hand (see Fig. 12). While the former aspect should lead to a higher hold-up, the latter accounts for a faster removal of the droplets and counterbalances it. Fig. 13 finally shows velocity vectors and contours of the axial and radial velocity in the organic phase. The typical vortices between the stators in the continuous phase are visible [22]. It is clear from Fig. 13 that the velocity vectors in the organic phase are directed to the bottom along the path of the RTIL. Therefore, the higher organic phase velocity with

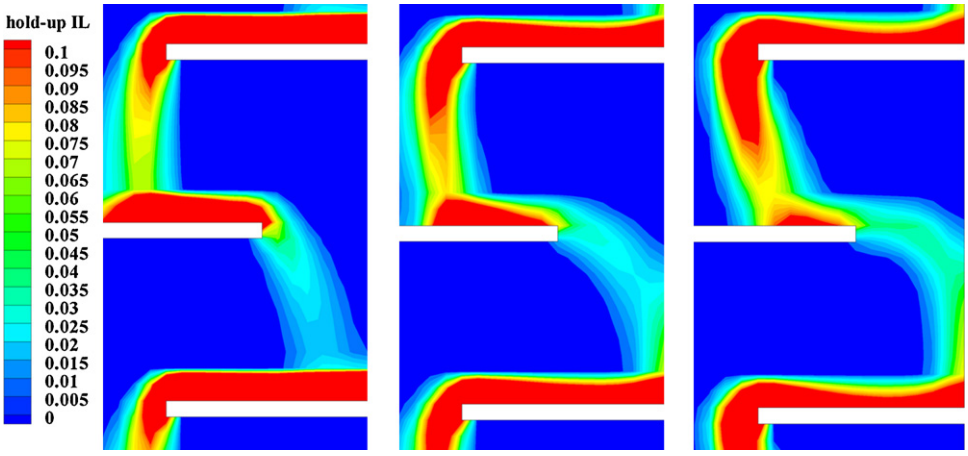

Fig. 10. Simulated hold-up, as a function of rotation speed (280–562–800 rpm) at flux 3.7 m^3/m^2 h, scaled from 0% to 10% volume fraction of the RTIL.

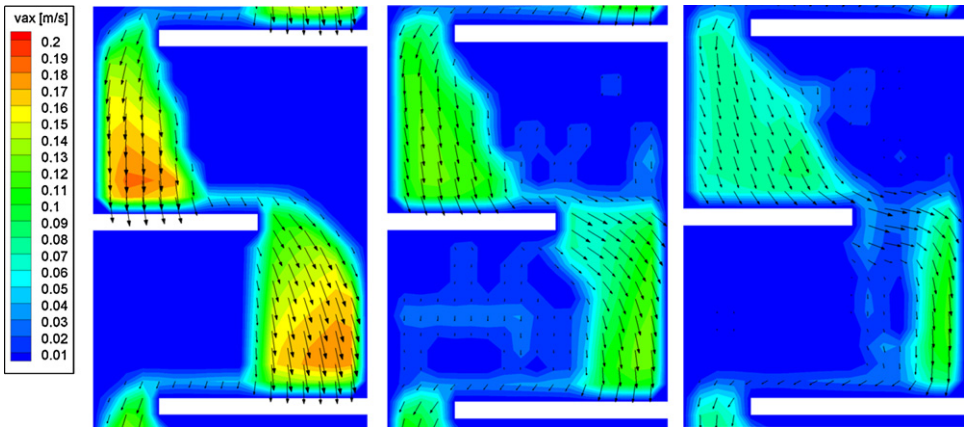

Fig. 11. Simulated velocity contours (axial velocity) and vectors of the RTIL as a function of rotation speed (280–562–800 rpm) at flux 3.7 m^3/m^2 h.

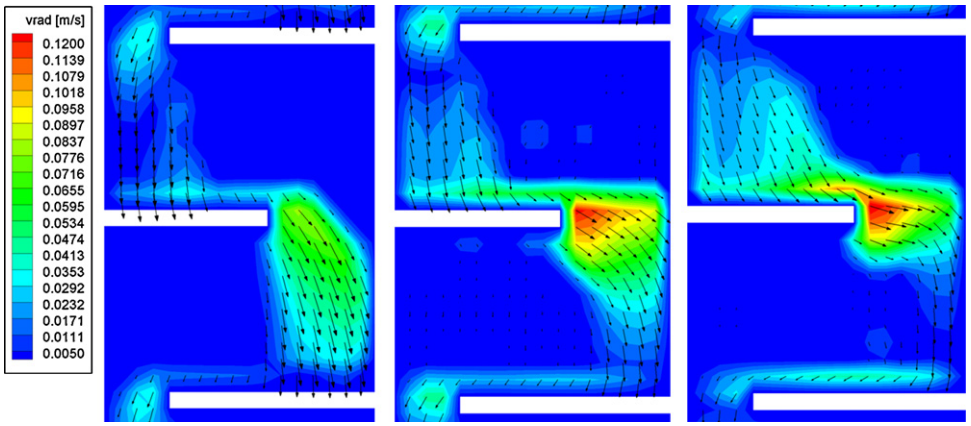

Fig. 12. Simulated velocity contours (radial velocity) and vectors of the RTIL as a function of rotation speed (280–562–800 rpm) at flux 3.7 m^3/m^2 h.

increasing rotor speed, also helps to carry out the RTIL droplets more easily. A comparison between the velocities in the RTIL phase (Figs. 11 and 12) and the organic phase (Fig. 13) shows the huge differences. The velocity in the RTIL phase is almost one order of magnitude higher than in the organic phase because of the big density difference and the small hold-up. Furthermore, the increasing rotor speed influences the organic phase velocities much more (see Figs. 11–13). The same trends are obvious for the higher fluxes (8.2, 10.5 m/h) and only results of the dispersed phase hold-up at 8.2 m/h are plotted in Fig. 14, where a higher overall hold-up is visible.

The numerical hold-up results are summarized and compared to the experimental hold-up results in Fig. 15. The experimental trend for the low flux (3.7 m/h) can be confirmed in the simulations. An increasing rotor speed results in a decreasing hold-up. The deviations between experimental and simulated data are small for the lower flux. In summary, the CFD simulations confirms the unexpected hold-up behavior at low flux and provide some explanation approaches, which are the path of the RTIL through the compartment and the velocities in the organic and RTIL phase.

However, the CFD model fails to predict the expected hold-up result at the higher fluxes (8.2, 10.5 m/h, red dots in Fig. 15). On the one hand, the hold-up is not increasing with higher flux as much as in the experiments, on the other hand, the CFD model cannot predict the "usual" behavior at the higher flux (8.2, 10.5 m/h), but it

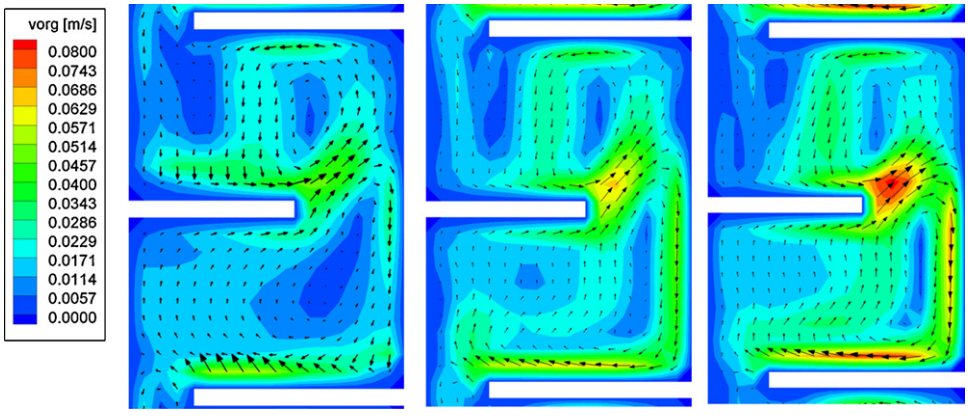

Fig. 13. Simulated velocity contours (axial and radial velocity) and vectors of the organic phase as a function of rotation speed (280–562–800 rpm) at flux 3.7 m^3/m^2 h.

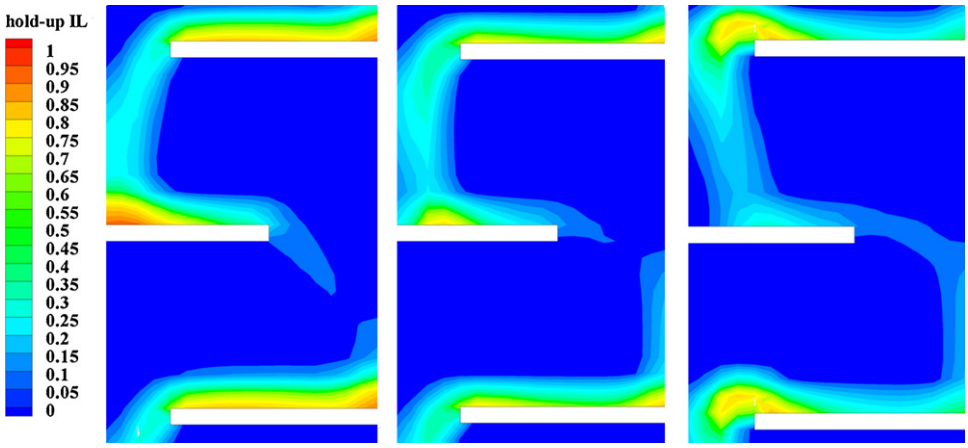

Fig. 14. Simulated hold-up of the RTIL as a function of rotation speed (280–562–800 rpm) at flux 8.2 m^3/m^2 h.

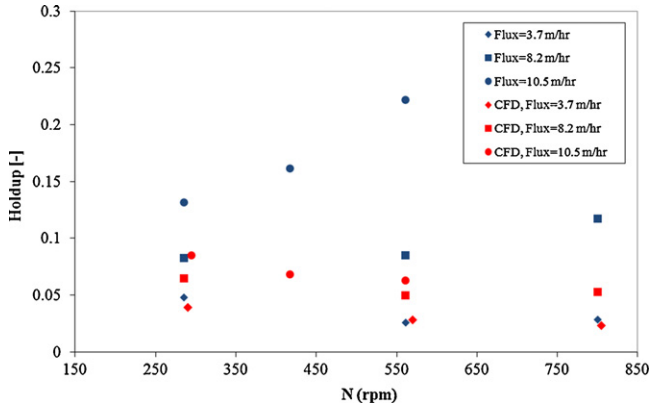

Fig. 15. Comparison simulated and experimental hold-up as a function of rotation speed and fluxes, original basic drag law (Eq. (7)).

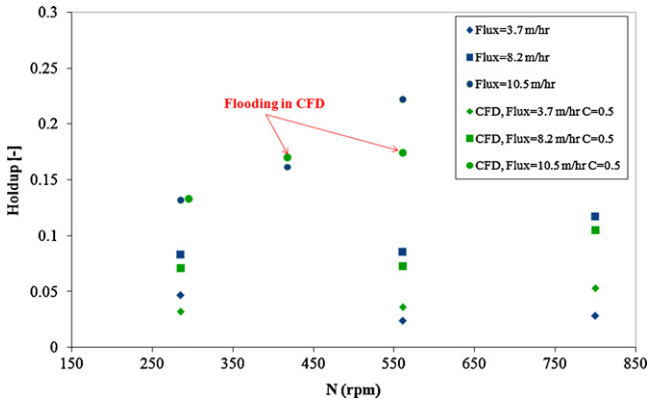

Fig. 16. Comparison simulated and experimental hold-up as a function of rotation speed and fluxes, modified drag law (Eq. (21)).

still predicts the same trend of decreasing hold-up as before. That is why a modified drag law was adopted that takes into account the effect of turbulence. It is based on a modified viscosity term in the relative Reynolds number and was also applied by Kerdouss et al. [36]. A model parameter was introduced in Eq. (11) to account for the effect of the turbulence in reducing slip velocity [36],

$$\mathrm{Re} = \frac{\rho_c \left|\vec{u}_d - \vec{u}_c\right| d_d}{\mu_c + C\mu_{t,c}} \tag{21}$$

where μ_t is the turbulent viscosity and C was set to 0.5. The predicted hold-up results for the modified drag law are summarized and compared to the experimental hold-up results in Fig. 15. Now it is visible that the hold-up is increasing with higher stirrer speeds. The deviations are now higher at the lowest flux but the prediction is much better at the higher fluxes (8.2, 10.5 m/h). At the highest flux, flooding occurs in the simulations at 420 and 560 rpm. This is probably caused by the fact that the column is almost operated at flooding for the highest flux. Therefore, the volume fractions cannot be compared for these two stirrer speeds (see Fig. 16). The simulated hold-up for the higher flow rates using the modified drag law (Eq. (21)) are finally shown in Figs. 17 and 18. It is visible that the hold-up is now increased along the path of the IL through the compartments due to a higher drag force at higher stirrer speeds. Therefore, by means of the modified drag law, it is possible to predict the hold-up results at the higher fluxes. In the present case, the value for C is an engineering estimate. One could obtain better results for each operating point if this factor is fitted.

There are some other possibilities to improve the CFD model for an even better prediction of the hydrodynamics and hold-up in the column. Only d_{32} of the drop size distribution was measured in the experiments in one compartment. Therefore, in the present work, a two-fluid model was applied using the constant d_{32} from experiments. In the real column this d_{32} is probably not constant, but could change with column height due to coalescence and breakage of the droplets and could also vary in each single extraction compartment. Usually, the small droplets are encountered near the stirrer, where breakage occurs, while the bigger droplets accumulate under the stators. A coupled CFD-population balance model (PBM) could take coalescence and breakage into account [27]. Furthermore, information about the drop size distribution could also improve the simulation results, when a multi-fluid model is applied as in Tomiyama and Shimada [37], where up to N fluids of the dispersed phase with different drop sizes are applied. Previous research could show that errors are introduced in a two-fluid model, where these size-specific velocities are not taken into account [27]. However, the current research still focuses on coupled CFD-PBM multi-fluid models, which are still under development (e.g. [27,38]). Other modeling possibilities would be to apply an enhanced wall treatment for the wall bounded turbulent flow or to vary the turbulence model. However, some test simulations applying an enhanced wall treatment together with a fine near-wall meshing did not deliver better results, but lead to convergence problems and a huge increase in CPU time.

There is also a need for future measurements with modern equipment e.g. the phase-doppler anemometer, which could provide the local drop size, volume fraction and droplet velocity in one extraction compartment for a better local comparison and a further improvement of the computational models. In the present

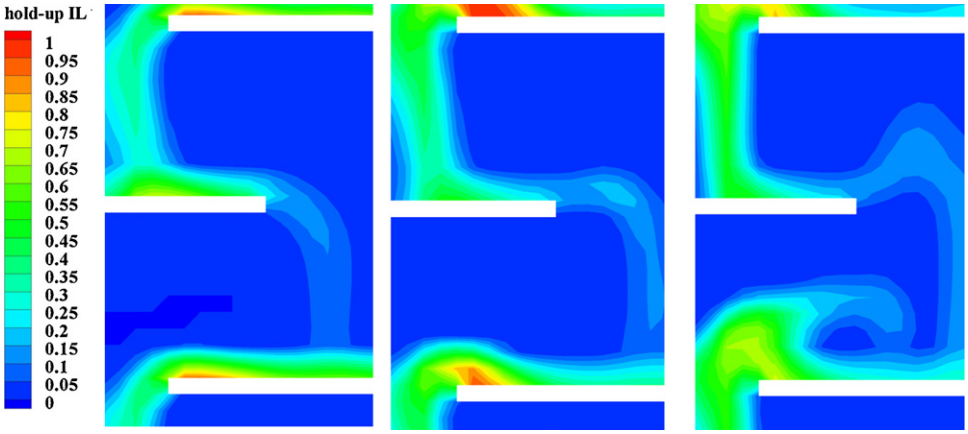

Fig. 17. Simulated hold-up of the RTIL as a function of rotation speed (280–562–800 rpm) at flux 8.2 m^3/m^2 h, modified drag law (Eq. (21)).

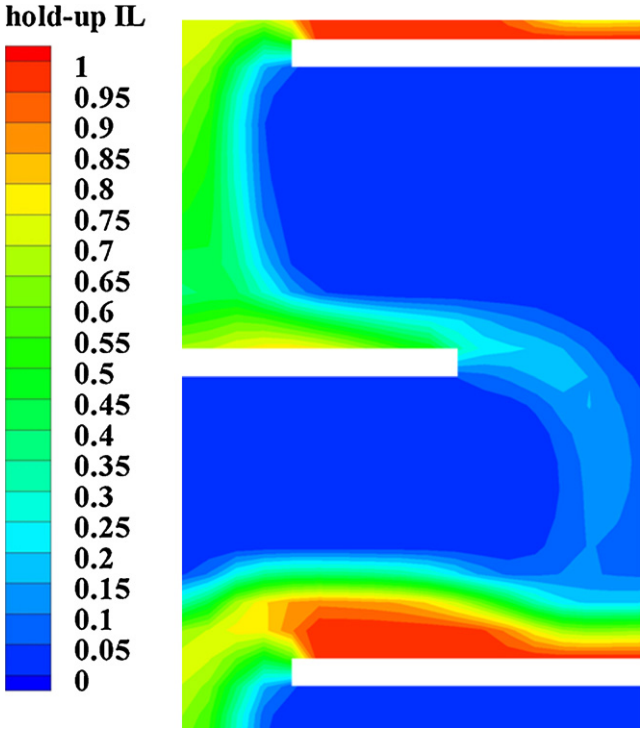

Fig. 18. Simulated hold-up of the RTIL as a function of rotation speed (280 rpm) at flux 10.5 m^3/m^2 h, modified drag law (Eq. (21)).

case, the hold-up was measured by taking 250 ml samples of the column content through sample ports. Since the droplets are not finely dispersed everywhere in the compartment, but move or even fall down mainly through the middle of the compartment and accumulate above stirrer and stators, small errors could be introduced in the measurements.

5. Conclusions

The RTIL 4-methyl-N-butyl-pyridinium tetrafluoroborate ([4-mebupy]BF_4) was tested as a solvent for the extraction of toluene from toluene/n-heptane in a rotating disc contactor. Hydrodynamic characteristics as Sauter mean diameters and hold-up were measured for different total fluxes and stirrer speeds. Unexpected behavior for the hold-up was observed in experiments when the RTIL was applied as solvent. At lower fluxes, the hold-up first decreased with increasing rotor speed, at a certain rotor speed, no influence of the rotor speed could be distinguished and, finally, with increasing rotor speed the hold-up increased as expected. With increasing fluxes this behavior diminished. At a certain flux an increase of the rotor speed resulted only in an increase of the hold-up. This phenomenon can be explained by the existence of three operational regimes for a rotating disc contactor; which clearly depend on flux and on rotor speeds.

Euler–Euler simulations of the two-phase flow were carried out in the framework of the commercial CFD software Fluent to investigate the unexpected hold-up behavior. The numerical hold-up results were compared to the experimental profiles. The experimental trend for the low fluxes could be confirmed in the simulations. The simulation results for the low fluxes match the experimental hold-up results. The hold-up anomalies at low fluxes could be explained by the unusual path of the RTIL droplets and the velocity fields in both liquid phases. The CFD model could also predict the hold-up result at the higher fluxes when a modified drag law was applied. Possible reasons for the deviations were discussed and some further model improvements as multi-fluid CFD models and coupled CFD-population balance models were given. The work shows, that CFD can be used for reasonable engineering predictions of the hydrodynamic characteristics and can provide an insight into hydrodynamic phenomena even for extreme examples as in the present RTIL extraction.

Acknowledgements

C. Drumm and H.-J. Bart would like to thank the Deutsche Forschungsgemeinschaft (DFG) for the financial support.

S.A.F. Onink, G.W. Meindersma and A.B. de Haan would like to express their gratitude to BASF for the financial support.

References

[1] J.G. Huddleston, H.D. Willauer, R.P. Swatloski, A.E. Visser, R.D. Rogers, Room temperature ionic liquids as novel media for 'clean' liquid–liquid extraction, Chem. Commun. (Cambridge, U.K.) 16 (1998) 1765–1766.
[2] F. Kubota, Application of ionic liquids to solvent extraction, Solvent Extr. Res. Dev., Jpn. 13 (2006) 23–36.
[3] G.W. Meindersma, A.B.d. Haan, Conceptual process design for aromatic/aliphatic separation with ionic liquids, Chem. Eng. Res. Des. 86 (2008) 745–752.
[4] M.L. Dietz, Ionic liquids as extraction solvents: where do we stand? Sep. Sci. Technol. 41 (2006) 2047–2063.
[5] S.H. Hamid, M.A. Ali, Comparative study of solvents for the extraction of aromatics from naphtha, Energy Sources 18 (1996) 65–84.
[6] https://www.uop.com/objects/55%20Sulfolane.pdf, in 2008.
[7] R. Krishna, A.N. Goswami, S.M. Nanoti, B.S. Rawat, M.K. Khanna, J. Dobhal, Extraction of aromatics from 63 to 69 °C naphtha fraction for food grade hexane production using sulpholane and NMP as solvents, Indian J. Technol. 25 (1987) 602–606.

[8] S.T. Anjan, Ionic liquids for aromatic extraction: are they ready? Chem. Eng. Prog. 102 (2006) 30–39.
[9] G.W. Meindersma, A. Podt, A.B. de Haan, Selection of ionic liquids for the extraction of aromatic hydrocarbons from aromatic/aliphatic mixtures, Fuel Process. Technol. 87 (2005) 59–70.
[10] P.P. Bailes, Hydrodynamic behavior of packed, rotating-disk and Kühni liquid–liquid-extraction columns, Chem. Eng. Res. Des. 64 (1986) 43–55.
[11] L. Blaiej, M. Vajda, S. Bafrncovd, Hydrodynamic properties of rotary-disc extractor, Chem. Papers 32 (1978) 314–327.
[12] M.S. Kamath, M.G.S. Rau, Prediction of operating range of rotor speeds for rotating disc contactors, Can. J. Chem. Eng. 63 (1985) 578–584.
[13] J.C. Godfrey, M.J. Slater, Liquid–Liquid Extraction Equipment, Wiley, 1994.
[14] E. Moreira, L.M. Pimenta, L.L. Carneiro, R.C.L. Faria, M.B. Mansur, C.P. Ribeiro Jr., Hydrodynamic behavior of a rotating disc contractor under low agitation conditions, Chem. Eng. Commun. 192 (2005) 1017–1035.
[15] A.A. Murakami, Dispersed phase holdup in a rotating disc extraction column, Int. Chem. Eng. 18 (1978) 16–22.
[16] G.W. Meindersma, G.S. Vos, M.B. Klaren, A.B. De Haan, Evaluation of contactor performance for extraction with ionic liquids, in: International Solvent Extraction Conference, Beijing, 2005, pp. 35–741.
[17] S.A.F. Onink, G.W. Meindersma, A.B.d. Haan, Ionic liquids in extraction operations: comparison of rotating disc contactor performance between [4-mebupy]BF4 and sulfolane® for aromatics extraction, in: International Solvent Extraction Conference, Tucson, USA, 2008, pp. 1337–1342.
[18] G.W. Stevens, T.C. Lo, M.H.I. Baird, Extraction, liquid–liquid, in: Kirk-Othmer Encyclopedia of Chemical Technology [Electronic version], John Wiley & Sons Inc., Weinheim, 2007, 1-62.
[19] G.W. Meindersma, A. Podt, A.B.d. Haan, Ternary liquid–liquid equilibria for mixtures of an aromatic an aliphatic hydrocarbon 4-methyl-N-butylpyridinium tetrafluoroborate, J. Chem. Eng. Data 51 (2006) 1814–1819.
[20] G. Modes, H.J. Bart, CFD simulation of nonideal dispersed phase flow in stirred extraction columns, Chem. Eng. Technol. 24 (2001) 1242–1245.
[21] W.Y. Fei, Y.D. Wang, Y.K. Wan, Physical modelling and numerical simulation of velocity fields in rotating disc contactor via CFD simulation and LDV measurement, Chem. Eng. J. (Amsterdam, Netherlands) 78 (2000) 131–139.
[22] C. Drumm, H.-J. Bart, Hydrodynamics in a RDC extractor: single and two-phase PIV measurements and CFD simulations, Chem. Eng. Technol. 29 (2006) 1297–1302.
[23] R. Rieger, S. Weiss, G. Wigley, H.-J. Bart, R. Marr, Investigating the process of liquid–liquid extraction by means of computational fluid dynamics, Comput. Chem. Eng. 20 (1996) 1467–1475.
[24] T. Haderer, CFD Simulation der Hydrodynamik einer gerührten Extraktionskolonne und Vergleich mit experimentell ermittlen hydrodynamischen Kenngrößen, TU Graz, Graz, 2004.
[25] T. Haderer, R. Marr, S. Martens, M. Siebenhofer, Bestimmung auslegungsrelevanter hydrodynamischer Kenngrößen einer RDC-Extraktionskolonne mit CFD, Chem. Ing. Tech. 77 (2005) 1055.
[26] F. Wang, Z.-S. Mao, Numerical and experimental investigation of liquid–liquid two-phase flow in stirred tanks, Ind. Eng. Chem. Res. 44 (2005) 5776–5787.
[27] C. Drumm, M. Attarakih, H.-J. Bart, Coupling of CFD with DPBM for an RDC extractor, Chem. Eng. Sci. 64 (2009) 721–732.
[28] Fluent Inc., Fluent's users guide, Lebanon, 2006.
[29] A. Kumar, S. Hartland, Prediction of drop size in rotating-disk extractors, Can. J. Chem. Eng. 64 (1986) 915–924.
[30] E.Y. Kung, B.B. Beckman, Dispersed-phase holdup in a rotating disk extraction column, AIChE J. 7 (1961) 319–324.
[31] S.S. Sarkar, C.R. Phillips, Characterization of hydrodynamic parameters in rotating-disk and Oldshue-Rushton columns – hydrodynamic modeling, drop size, hold-up and flooding, Can. J. Chem. Eng. 63 (1985) 701–709.
[32] H.J.J.A. Vermijs, H. Kramers, Liquid–liquid extraction in a "rotating disc contactor", Chem. Eng. Sci. 3 (1954) 55–64.
[33] M.S. Kamath, K.L. Rao, R. Jayabalou, P.K. Karanth, M.G.S. Rau, Holdup studies in a rotary disk contactor, Indian J. Technol. 14 (1976) 1–5.
[34] A.G. Kasatkin, S.Z. Kagan, V.G. Trukhanov, Hold-up of rotating disk contactors, J. Appl. Chem. USSR 35 (1962) 1903–1910.
[35] A.M.I. Al-Rahawi, New predictive correlations for the drop size in a rotating disc contactor liquid–liquid extraction column, Chem. Eng. Technol. 30 (2007) 184–192.
[36] F. Kerdouss, A. Bannari, F. Proulx, R. Bannari, M. Skrga, Y. Labrecque, Two-phase mass transfer coefficient prediction in stirred vessel with a CFD model, Comput. Chem. Eng. 32 (2008) 1943–1955.
[37] A. Tomiyama, N. Shimada, A numerical method for bubbly flow simulation based on a multi-fluid model, J. Pressure Vessel Technol. 123 (2001) 510–516.
[38] E. Krepper, D. Lucas, T. Frank, H.-M. Prasser, P.J. Zwart, The inhomogeneous MUSIG model for the simulation of polydispersed flows, Nucl. Eng. Des. 238 (2008) 1690–1702.
[39] C.L. Yaws, Chemical Properties Handbook: Physical, Thermodynamic, Environmental, Transport, Safety, and Health Related Properties for Organic and Inorganic Chemicals, McGraw-Hill, New York, 1999.